

# Predictive Numerical Modeling of Foreign Object Damage

Pierangelo Duó and David Nowell

*University of Oxford, Department of Engineering Science,  
Parks Road, Oxford OX1 3PJ, UK*

## Abstract

*During service aircraft engines may suffer foreign object damage (FOD) from ingestion of small hard particles and then are subjected to a range of HCF-LCF cycles. Manufacturers are seeking to improve the FOD tolerance of engines at the design stage and thereby reduce the costs of ownership. A design methodology is therefore required with which to assess the loss of fatigue strength resulting from FOD on blades or vanes. This work describes progress in the prediction of the residual stresses left from the impact in a specimen which resembles a compressor blade. The FE package LS-DYNA has been used to analyse the problem. Initially different material models were considered, each including a strain rate dependence, and a calibration based on a tensile test was performed. The Bamman Damage (Mat 52) was then chosen and used in the numerical model of impact on an aerofoil leading edge. The model has proved capable of recreating the damage geometry and gives a valuable insight into the likely residual stress distribution around the notch. A subsequent fatigue analysis of the impacted blade has been run using the same material model. A methodology based on a posteriori analysis and comparison with post-impact fatigue experiments has been used to confirm the results obtained.*

Keywords: *Foreign Object Damage (FOD), Impact Modeling, Residual Stresses, Bamman Damage material model.*

---

Corresponding author: Pierangelo.Duo@eng.ox.ac.uk

## 1. Introduction

Gas turbine engines can often be subjected to impact from external bodies ingested during landing or takeoff. When birds are ingested the damage caused is called “soft body” impact whereas when stones, pieces of metal or other small compact debris enter the engine it is called “hard body” ingestion and the damage is identified as Foreign Object Damage, or FOD. There is a need to improve FOD tolerance in order to decrease the cost of ownership. The ingested objects can hit the compressor blades which are, in general, the part of the engine most susceptible to FOD, due to their position and high rotational speed. FOD has a particularly severe effect in the case of high cycle fatigue applications where it leads to a decrease in the fatigue strength. In particular it has been demonstrated (Mall et al. 2001) that failure occurs due to the combination of three factors: geometric stress concentration in a V-notch or similar geometry, micro-structural damage, and residual stress effects. Previous work (Nowell et al. 2003) demonstrated a decrease of the damaged fatigue strength as a function of the size of the FOD notch. However this parameter does not fully characterise the loss of fatigue performance since it does not consider the residual stress effect.

Different techniques have been used in the past to reproduce FOD in the laboratory. Early approaches used a swinging pendulum or quasi-static indenter. These approaches will almost certainly not generate a realistic residual stress field as the strain rates will be much lower than a real impact. More recent work has attempted to reproduce FOD more closely using a gas gun

apparatus in order to generate the strain rates required (Nowell et al. 2003, Duó et al. 2003). As part of the current investigation, a number of experiments have been performed using a gas gun in order to investigate the effect of varying the leading edge radius, the wedge angle, or the impact angle. In general the objective of recent work has been to investigate the effects of missile size, shape and kinetic energy on the size of inelastically deformed zone and the magnitude of the residual stress. A correlation with short crack threshold theory (Hudak and Chell, 1999) has been introduced (Nowell et al., 2003).

The current work focuses on the prediction of the residual stress present after the impact. These stresses are difficult to measure and modeling is therefore required. The explicit LS-DYNA code (Livermore 2001) was identified as an appropriate tool. Due to the short duration of the event a visco-plastic material model with strain rate hardening was used. The MPI option was used to enable parallel computation using the \*CONTROL\_PARALLEL card. This enabled effective use of up to 8CPUs on a parallel supercomputer cluster at Oxford (OSCAR/OSWELL).

## 2. Methodology

### 2.1 Material models

In this study the analysis was performed using LS-DYNA and an investigation of two different material models was undertaken. The Bamman Damage material model (Bamman 1993) MAT 52 in LS-DYNA, was considered to be the most suitable and was used for subsequent modeling. Typically the material model is a functional relationship between the values of stress, strain, strain rate and temperature such as:

$$\sigma = \sigma (\dot{\varepsilon}_p, \varepsilon_p, T) \quad (1)$$

for a path independent material or:

$$\left( \frac{d\sigma}{d\varepsilon} \right) = \varphi(\sigma, \dot{\varepsilon}, T) \quad (2)$$

for path dependent materials. Whichever material model is chosen, values must be selected for the parameters in the model. Here we make the assumption that, for any state of three-dimensional stress, the strain, strain rate and stress can be reduced to an equivalent uniaxial stress state (Noble et al. 1999). This enables material parameters to be identified by testing specimens of the blade material in a split Hopkinson-bar apparatus, Macdougall et al. (1999).

### 2.3. Damage and failure

In FOD the relative velocity between the blade and ingested object is predominantly due to blade rotation and of the order of 200-300 m/s. Significant plastic deformation occurs in the blade following the impact and this can lead to a loss of material, generating a notch. A full analysis of the problem, therefore, requires not only a valid constitutive relation but also the inclusion of some form of failure criterion for the material. The Bamman damage model is based on a damage mechanics approach, where the evolution and coalescence of voids is the mechanism of failure of the material. In this model, the growth of a damage parameter is governed by a relationship between the current state of damage, the internal pressure and the effective stress. In implementing the model, the \*ERODING\_SURFACE\_TO\_SURFACE option card was employed to remove failed elements and speed up the calculation. If failed elements are not removed in this way, an unrealistic deformation is predicted after an extremely long calculation time (e.g. 40 hours using 8 CPUs on OSCAR).

### 3. Impact Analysis

#### 3.1. The model

The modeling of the blade-like specimens used in the experiments started from the CAD model reproducing the complete geometry, originally used for manufacturing. This model was sectioned with a plane parallel to the platform, to obtain the cross section surface (Fig.1). A prismatic model was then built by extruding this surface for a length necessary to minimise boundary effects during the impact (> 15X the largest impact damage). The projectile was a 3.22 mm cube. In order to contain the number of elements required, this was meshed with a one-way graduated element length for each of the three sides (0.050 to 0.298mm), where the minimum element size at the corner hitting the blade (Fig.2). The cube was modeled as linear elastic (steel) with no failure criterion, since the cubes used in the experiment were found to be essentially undamaged after impact. The geometry of the blade studied had a very fine leading edge radius, which needed to be modeled with a reasonable degree of refinement. The finest mesh used for the specimen had a minimum element size of 0.035mm, resulting in about 500,000 degrees of freedom for the largest leading edge radius geometry. The cube model was launched against the specimen using an imposed initial velocity of 250 m/s. The specimen model does not have any boundary conditions, other than non-reflective boundaries on the top and bottom surfaces of the blade section. These were used, since the boundaries in the model were much nearer the impact site in the real specimen and unwanted wave-reflections would otherwise occur in the model.

Each specimen model was then rotated in the X-Y plane by an angle “ $\beta$ ” corresponding to the relevant experimental set up. This angle is defined as that between the direction of travel of the cube and the mid-plane of the specimen in Fig.3, where the leading edge radius is indicated by “R” and the wedge angle by “ $\alpha$ ”. For the datum series of experiments, the impact angle was 50 degrees. The cube was positioned in front of the leading edge in a ‘point-first’ orientation with an overlap,  $x_c$ , of 0.65mm (Fig.4). This dimension represented the average value used in the experiments (Nowell et al., 2003) and is similar to values found in the literature (Gravett et al. 1999).

#### 3.2. Dynamic calculation

Calculation in explicit code is performed in discrete time-steps of size:

$$\Delta t = \frac{l_e}{c} \quad (3)$$

where  $l_e$  = length of each finite element,  $c$  = wave speed through the material. The wave speed is defined as:

$$c = \sqrt{\frac{E}{\rho}} \quad (4)$$

where  $E$  = Young’s Elastic Modulus,  $\rho$  = density, giving  $c \cong 5000$  m/s for the Ti6Al4V material used in the test. Therefore

$$\Delta t = l_e \sqrt{\frac{\rho}{E}} \quad (5)$$

and since  $l_e$  and  $E$  are constant,

$$\Delta t \propto \sqrt{\rho} \quad (6)$$

Due to the high strain rates experienced during the event, attempts to apply mass scaling to reduce the effective time of the calculation were not thought likely to give accurate results. This assumption was borne out in practice and mass scaling was not, therefore, applied.

### 3.3 Results

The numerical results obtained from LS-DYNA show that impact was a few microseconds in duration. A number of features of the impacted specimen were clearly reproduced in the simulation, including

- 1) in all cases, a V-shaped notch was produced in the model, similar in size and shape to that in the experiment;
- 2) different geometries and alignments of specimen produced different notch geometries and, in particular, markedly different residual stress profiles in the neighbourhood of the impact location.

### 3.4. Discussion of the simulation

As mentioned above, simulations were run on the different specimen geometries used in the experiments. Different analyses were also run on the datum specimen geometry, changing the impact angle. The geometric damage resulting from the impact was essentially a V-notch in all the cases examined. A particular area of interest was the residual stress distribution around the impact site. Such stresses are thought to play a key role in encouraging or preventing fatigue crack initiation (Mall et al., 2001). Residual stresses were obtained by running the simulation after the impact until stresses at the impact site had stabilised to within a prescribed tolerance. Non-reflective boundary conditions were clearly important in achieving this.

We discuss first the analysis of the impact on the datum specimen at 50 degrees. The residual stress component in the axial ( $z$ ) direction is chosen for discussion, since this is most likely to influence fatigue crack initiation. Overall, the  $\sigma_{zz}$  residual stress component is tensile on the front (impact) face of the specimen and compressive on the back. However, some residual compression exists through the entire specimen thickness at the root of the notch (Fig.5). This may be clearly seen in the section, which is obtained using a cutting plane through the root of the notch, perpendicular to the leading edge. Stresses on this plane are important since it is where fatigue cracks are most likely to initiate. Fig.6 shows the fracture surface of a specimen after fatigue testing. The three lines drawn here are chosen to examine the predicted residual stress for further analysis. The residual stresses for this case are plotted (normalised with respect to the yield quasi-static point) in Fig.7, as a function of the notch root distance.

The influence of the 20 degree impact angle was also analysed and due to the more ‘nose-on’ impact there is more residual compression on the front of the blade and tensile on the back (Fig.8). This is expected to be less damaging for subsequent fatigue life. Further analyses were also run for the datum specimen. The impact at 50 degrees angle and 0.25mm leading edge radius was compared to a larger leading edge radius of 0.51 mm under the same impact conditions. Observation of the residual stresses shows that the maximum residual tensile stress occurs subsurface, corresponding to the quarter line position (a line half way between ‘front’ and ‘center’ in Fig.6). Normalised residual stresses for this case are plotted in Fig.9, as a function of the distance from the notch root.

## 4. Fatigue Analysis

The current version of LS-DYNA allows restarting of the analysis in implicit mode with the same material model used to perform the impact. Several full cycles of fatigue loading were therefore applied to the specimen after impact to check if any shakedown of residual stress occurred. The general approach follows that presented recently by Maker et al. (2003) and Patwardhan et al. (2003). In particular the card \*INTERFACE\_SPRINGBACK\_DYNA3D has been used. This allows an implicit spring-back simulation and is employed here to restart the analysis in implicit mode, loading the specimen under the cyclic fatigue load. The load was applied through displacement boundary conditions on both ends of the specimen cross-section, to give applied stresses representative of the real fatigue loading cycle. Preliminary investigations have shown encouraging results, predicting a decrease in residual stress levels. However further work is still required on this part of the analysis.

## 5. Conclusions

The comparison of different constitutive models has shown that only the use of an appropriate material model including the strain rate effects can adequately represent the impact event occurring at 250 m/s. In particular the distribution of residual stresses in impacted ‘blade-like’ specimens is significantly affected by the chosen model. The *distribution* of residual stresses is important in determining the origin of subsequent fatigue crack initiation. On the other hand, the *magnitude* of residual stresses and the shape of deformed geometry region are clearly important in defining the fatigue limit of the damaged component. It has been shown that the maximum residual stresses is not always at the notch root, but can occur a small distance inside the blade, usually close to the front (impact) surface. The notch root itself is generally in a zone of residual compression, which may suppress crack initiation there. Implicit analysis of fatigue loading subsequent to the impact, with the same material model, has shown that a degree of shakedown of the residual stress may take place.

## Acknowledgements

The authors wish to acknowledge the financial support of Rolls-Royce plc and the UK Ministry of Defence for the work described here.

## References

1. Bamman D.J., Chiesa M.L. Horstemeyer M.F. and Weingarten L.I. (1993) “*Failure in Ductile Materials using Finite Element Methods*” Chapter 1 in Structural Crahsworthiness and Failure, Ed. By N. Jones and T. Wierzbicki, Elsevier Applied Science, London.
2. Duó P., Nowell D., and Stewart I.F. (2003), “*The role of FOD in decreasing the residual fatigue strength of Ti6Al4V compressor blades*”, Proceedings of the 8<sup>th</sup> High Cycle Fatigue Conference, Monterey, CA.
3. Gravett Ph., Bellows, R. Duniyak T., Herrmann D. and Hudak S. Jr. (1999) “*The Foreign Object Damage Project of the PRDA V HCF Materials and Life Methods Program*” Proceedings of the 4<sup>th</sup> National Turbine Engine High Cycle Fatigue Conference, Monterey, CA.
4. Hudak S.J. Jr. and Chell G.G. (1999), “*A Damage Tolerance Approach to FOD Based on the ‘Worst Case Notch’ Concept*”, Proceedings of the 4<sup>th</sup> National Turbine Engine High Cycle Fatigue Conference, Monterey, CA.
5. Livermore Software Technologies Corporation (2001), LS-DYNA User’s Guide.

6. Maker B., Grimes R. Ashcraft C. “*Implicit Functionality in LS-DYNA v970*” 4<sup>th</sup> European LS-DYNA Users Conference, Ulm (Germany) 2003.
7. Mall S., Hamrick J.L.II, and Nicholas T. (2001), “*High cycle fatigue behavior of Ti–6Al–4V with simulated foreign object damage*”, Mechanics of Materials, Vol. **33**, Issue 11, Nov. 2001, pp.679-692.
8. Macdougall D.A.S. and Harding J. (1999), “*A constitutive relation and failure criterion for Ti6Al4V alloy at impact rates of strain*” Journal of the Mechanics and Physics of Solids, Vol. **47**, Issue 5, pp.1157-1185.
9. Noble J.P. Goldthorpe B. D., Church P. and Harding J. (1999) “*The use of the Hopkinson bar to validate constitutive relations at high rates of strain*”, Journal of the Mechanics and Physics of Solids, Vol. **47**, Issue 5, pp.1187-1206.
10. Nowell D., Duó P., and Stewart I.F. (2003), “*Prediction of fatigue performance in gas turbine blades after foreign object damage*” Int. Jnl Fatigue, Vol. **25**, pp.963-969.
11. Patwardhan V., Sambamoorthy B. Halder T. “*Simulation of proposed FMVSS 202 using LS-DYNA Implicit*” 4<sup>th</sup> European LS-DYNA Users Conference, Ulm (Germany) 2003.

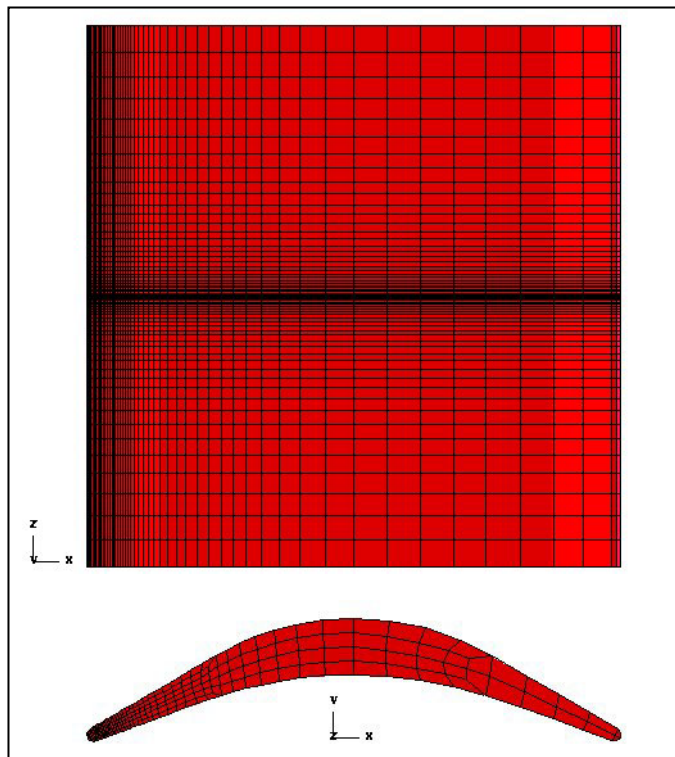


Figure 1. Mesh of “blade-like” specimen and cross section (datum specimen).

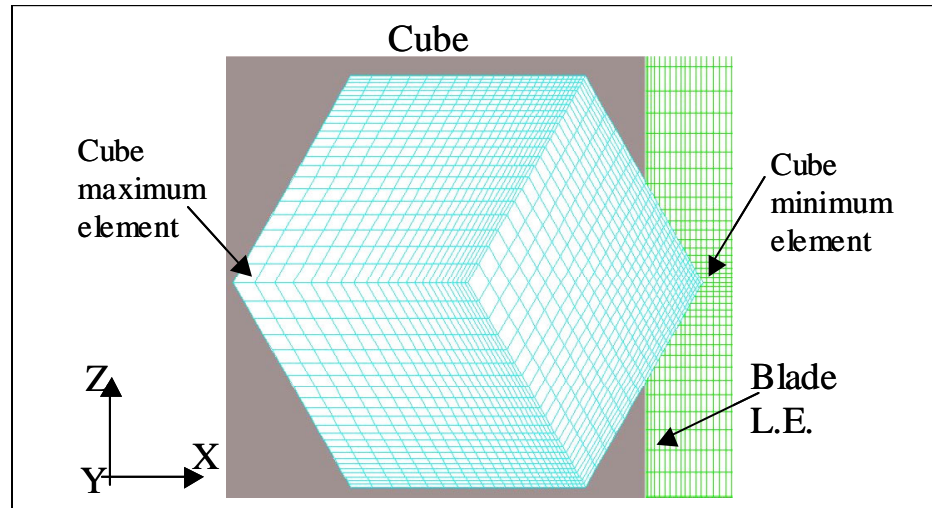


Figure 2. Mesh of the cube, showing position relative to the specimen.

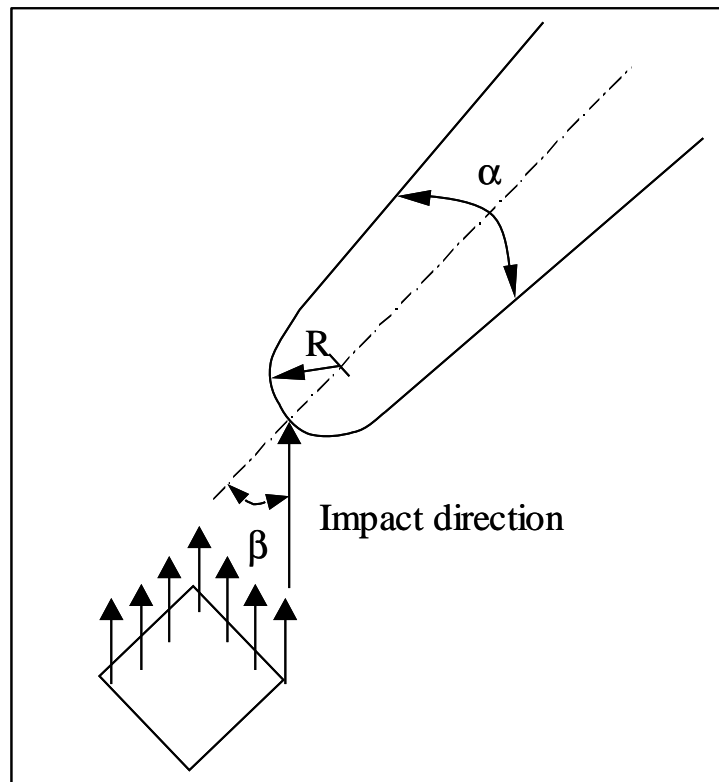


Figure 3. Diagram showing the impact geometry.

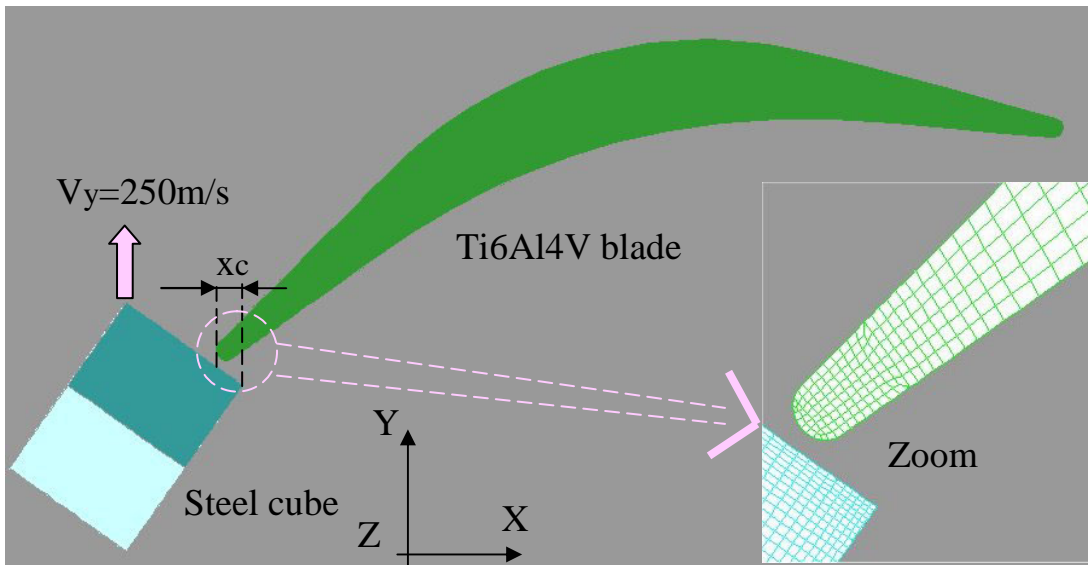


Figure 4. Impact geometry, showing overlap between cube and specimen.

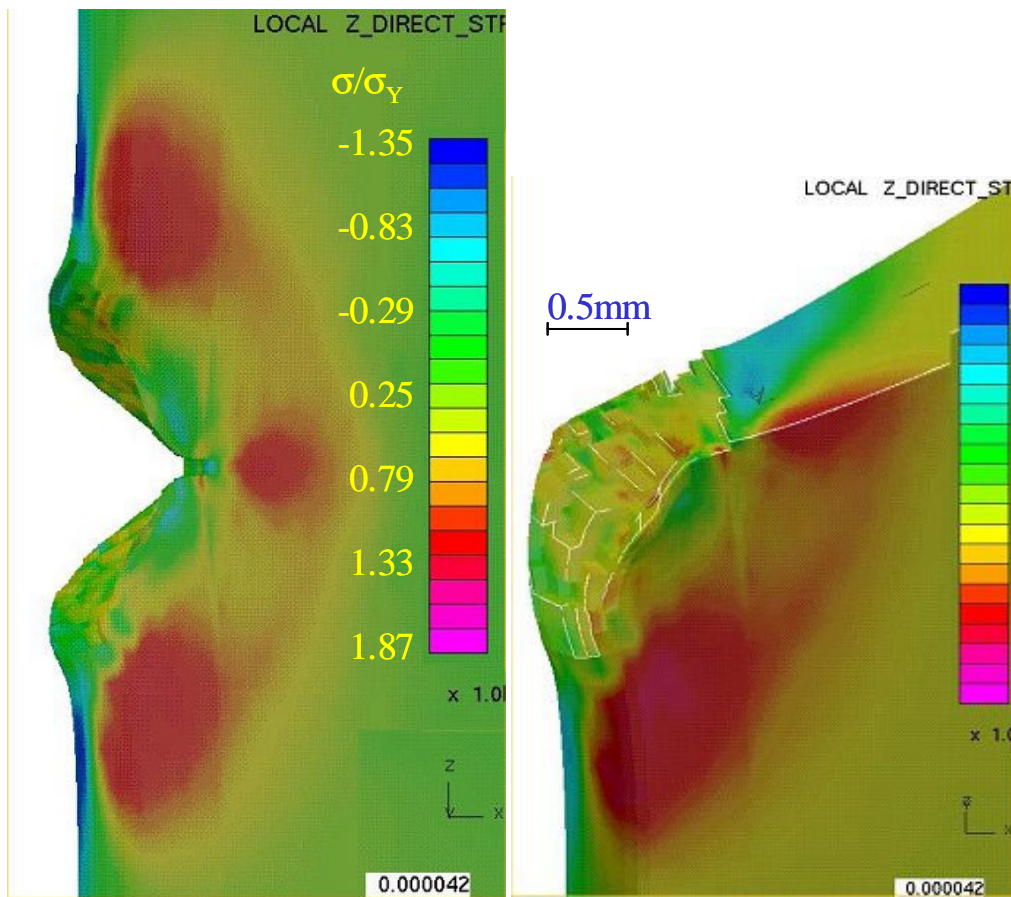


Figure 5. Impact results on the datum specimen,  $\beta=50$  degrees. Stress components show are  $\sigma_{zz}$  residual stresses.

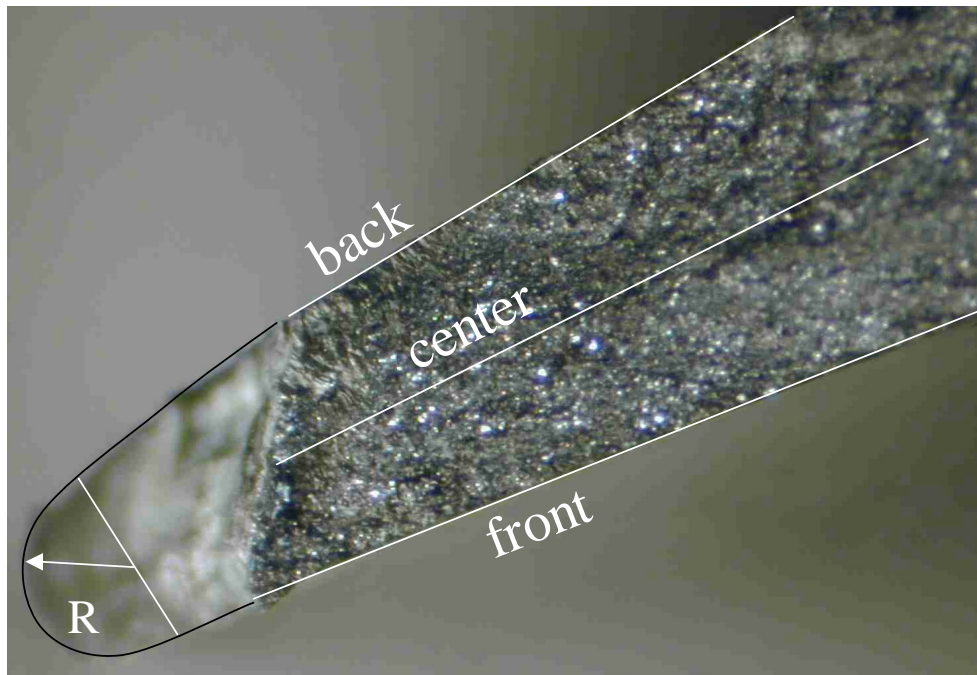


Figure 6. Fracture surface showing three lines where residual stress profiles are taken.

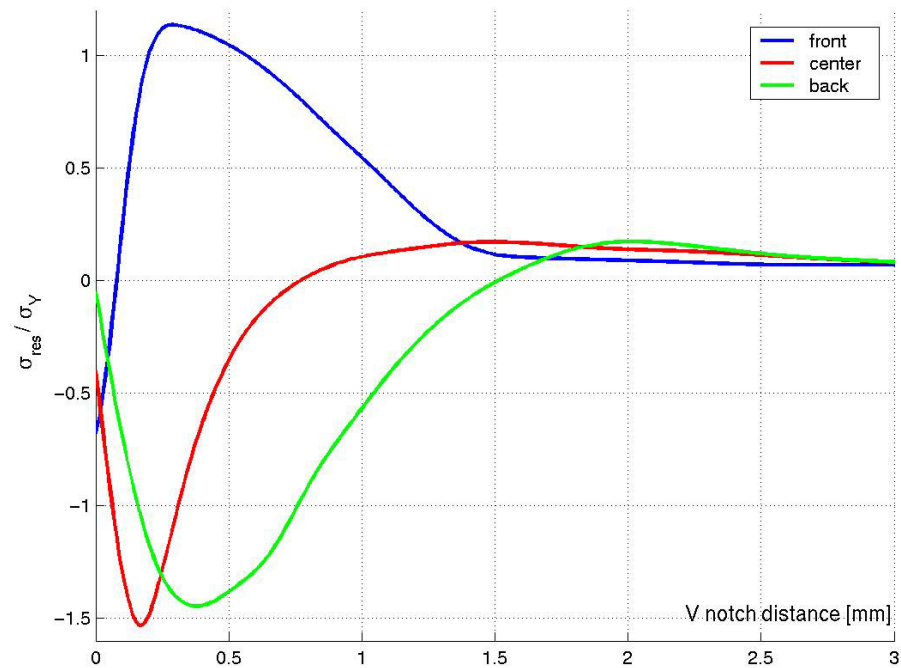


Figure 7.  $\sigma_{zz}$  residual stress components as a function of position from the notch root for the three different lines shown in Fig.6 ( $\beta=50$  degrees).

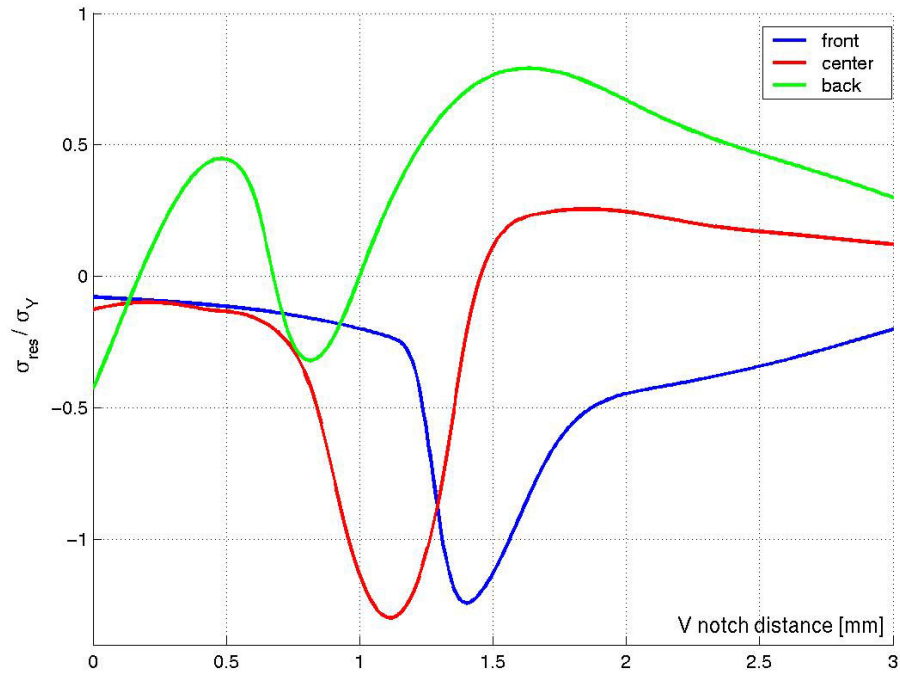


Figure 8.  $\sigma_{zz}$  residual stress components as a function of position from the notch root for the three different lines ( $\beta=20$  degrees).

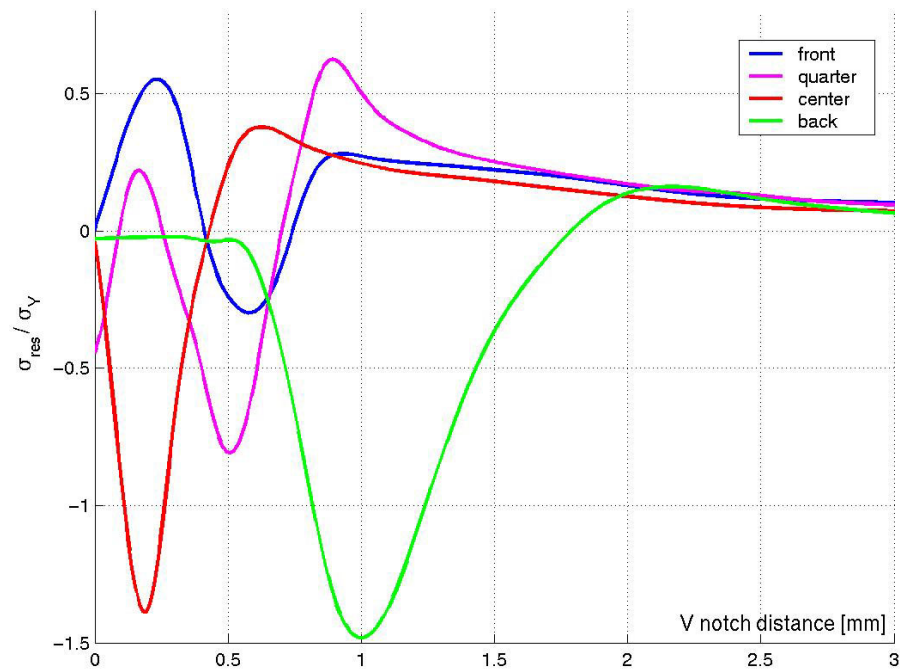


Figure 9.  $\sigma_{zz}$  residual stresses in the blade with 0.51mm leading edge radius.